

## International Conference on Computational Science, ICCS 2011

### Application of high-resolution methods in compositional simulation

Jiří Mikyška<sup>a</sup>, Abbas Firoozabadi<sup>b</sup>

<sup>a</sup>*Czech Technical University in Prague, Faculty of Nuclear Sciences and Physical Engineering, Department of Mathematics, Trojanova 13, 120 00 Prague, Czech Republic*

<sup>b</sup>*Reservoir Engineering Research Institute, 595 Lytton Ave, Palo Alto CA-94301, United States of America*

---

#### Abstract

Compositional simulation is an important tool in for evaluation of oil recovery and carbon sequestration. Several compositional models have been proposed in the past that are based on finite-difference, finite-volume or finite-element methods. These methods are typically of low order of approximation and suffer excessive numerical diffusion. These deficiencies can be significantly suppressed using the high resolution methods like mixed-hybrid and discontinuous Galerkin finite element methods. We have shown recently that these methods are much more sensitive to problem formulation than the conventional first-order methods. In this work we discuss several problems connected with application of high resolution schemes. These problems include formulation of boundary conditions, proper evaluation of phase fluxes, and formulation of the slope limiter in the discontinuous Galerkin method. The latter problem is common to all high resolution methods. We will present new examples of compositional simulations showing the advantages of our approach over the traditional first-order finite-volume schemes in single-phase and two-phase.

*Keywords:* two-phase flow, compositional simulation, high resolution methods, mixed-hybrid finite element method, discontinuous Galerkin method, slope limiter

---

#### 1. Introduction

Mathematical models of gas injection into a porous medium with species transfer between the phases are essential for solving problems of enhanced oil recovery and CO<sub>2</sub> sequestration. Injection of CO<sub>2</sub> into an oil reservoir may lead to complex behavior - e.g. the supercritical CO<sub>2</sub> can cause an originally single-phase hydrocarbon mixture to split into phases. The phase properties like density or viscosity depend significantly on pressure, temperature, and chemical composition of each phase. Because of these complexities, efficient and robust compositional simulation of two-phase flow in porous media remains a challenging problem.

The traditional approaches are based on the first-order finite difference or first-order finite volume schemes. To obtain a solution without spurious oscillations, upwinding techniques are used which lead to non-oscillating solutions suffering from enormous amount of artificial diffusion. Although the excessive numerical diffusion can be suppressed by sufficiently refining the mesh, this approach is not practical because the mesh refinement leads to computation of extremely large systems for many cells. With large number of smaller cells, the time steps are chosen to be very small to satisfy the time stability constraints. Consequently, mesh refinement is not effective in terms of the CPU time

---

*Email addresses:* [jiri.mikyska@fjfi.cvut.cz](mailto:jiri.mikyska@fjfi.cvut.cz) (Jiří Mikyška), [abbas.firoozabadi@yale.edu](mailto:abbas.firoozabadi@yale.edu) (Abbas Firoozabadi)

required to obtain sufficiently accurate results. Accuracy can be improved without excessive mesh refinement using the high resolution methods like the finite-element method, where one can increase accuracy of the solution by using higher-order polynomial approximation of the exact solution. In this paper we use a combined approach based on the mixed-hybrid finite element (MHFE) and discontinuous Galerkin (DG) finite element methods which are stabilized using a slope limiter. The MHFE yields high accuracy in flux evaluation while the DG provides a non-oscillating solution with substantially lower numerical diffusion in comparison with the first-order schemes. Moreover, the values of pressure at element centers provided by the MHFE can be used directly values for performing the flash calculations on element edges. The combined method was first proposed in [1] for single phase multicomponent flow and further extended to two-phase compositional flow in [2] and [3]. Later we have discovered several issues with problem formulation that were critical for the application of high resolution methods. Some of these issues have been discussed in [4]. In this paper, we offer some additional explanations and new examples demonstrating important features of the method.

The paper is structured as follows. In the first section, we review the problem formulation. Then, we describe the discretization of the system of equations. This involves discretization of the total flux using the MHFE, evaluation of the phase fluxes, discretization of the transport equations using the DG, and description of the slope limiting procedure. Finally, we present results of example computations showing efficiency and robustness of our method.

## 2. Model formulation

The two-phase transport of  $n_c$  components in porous media is described by the following set of balance equations

$$\phi \frac{\partial c z_i}{\partial t} + \nabla \cdot (c_o x_{oi} \mathbf{v}_o + c_g x_{gi} \mathbf{v}_g) = F_i, \quad i = 1, \dots, n_c, \quad (1)$$

where  $\phi$  is the porosity,  $c$  is the overall molar density,  $z_i$  is the overall mole fraction of  $i$ -th component,  $c_o$ ,  $c_g$ ,  $x_{oi}$  and  $x_{gi}$  are the oil and gas molar densities and oil and gas molar fractions, respectively,  $F_i$  describes distribution of the sources/sinks of the  $i$ -th component, and  $t$  denotes the time. In this work capillarity and diffusion are neglected. The formulation of the two-phase compositional problem including diffusion can be found in [5]. The temperature  $T$  is assumed to be constant. The phase velocities  $\mathbf{v}_o$  and  $\mathbf{v}_g$  are given by Darcy’s laws,

$$\mathbf{v}_\alpha = -\lambda_\alpha(S_\alpha) \mathbf{K}(\nabla p - \rho_\alpha \mathbf{g}), \quad \alpha \in \{o, g\}, \quad (2)$$

where  $\lambda_\alpha$  is the  $\alpha$ -phase mobility,  $\mathbf{K}$  is the permeable medium intrinsic permeability,  $p$  is the pressure,  $\rho_\alpha$  is the  $\alpha$ -phase density, and  $\mathbf{g}$  is the gravity acceleration vector. As capillarity is neglected, the pressures in both phases are the same. The viscosities in the mobility terms are estimated using the correlation of Lohrenz et al. [6]. Based on the concept of volume-balance (see [7]), the following pressure equation can be derived

$$\phi c_f \frac{\partial p}{\partial t} + \sum_{i=1}^{n_c} \bar{v}_i \nabla \cdot (c_o x_{oi} \mathbf{v}_o + c_g x_{gi} \mathbf{v}_g) = \sum_{i=1}^{n_c} \bar{v}_i F_i, \quad (3)$$

where  $c_f$  and  $\bar{v}_i$  denote the total fluid compressibility and the total partial molar volume of the  $i$ -th component, respectively. These coefficients can be evaluated using the pressure, temperature, and chemical composition (see [8] for details). The splitting of components between the phases is described by the following equations expressing local thermodynamic equilibrium

$$f_{oi}(x_{o1}, \dots, x_{on_c-1}, p; T) = f_{gi}(x_{g1}, \dots, x_{gn_c-1}, p; T), \quad i = 1, \dots, n_c, \quad (4a)$$

$$z_i = (1 - \nu)x_{oi} + \nu x_{gi}, \quad i = 1, \dots, n_c, \quad (4b)$$

$$\sum_{i=1}^{n_c} x_{oi} = \sum_{i=1}^{n_c} x_{gi} = \sum_{i=1}^{n_c} z_i = 1, \quad (4c)$$

where  $f_{oi}$  and  $f_{gi}$  represent fugacities of the  $i$ -th component in the respective phase, and  $\nu$  is the gas mole fraction. The phase molar densities  $c_\alpha$  are evaluated using the Peng-Robinson equation of state (PR-EOS) [9], [8]. The phase saturations (needed in (2)) are calculated from

$$S_o = \frac{c}{c_o}(1 - \nu), \quad S_g = \frac{c}{c_g}\nu. \quad (5)$$

The saturation constraint  $S_o + S_g = 1$  provides an additional expression

$$1 - c \left( \frac{1-v}{c_o} + \frac{v}{c_g} \right) = 0, \quad (6)$$

from which  $c$  can be evaluated independently of the transport equations (1). In the computations, the value of  $c$  is determined from equations (1) and the constraint equation (6) is used as a criterion for the selection of a time step.

### 3. Treatment of impermeable boundaries

We simulate two-phase compositional transport in a rectangular domain in which the gas or the supercritical fluid is injected in one corner and the mixture of oil and gas is produced in the opposite corner. The boundaries of the domain are impermeable. Although this is a standard setup of many simulations reported in the literature, it may be surprising that the formulation described above does not allow to enforce impermeability for both phases if the mixture is in two-phase. The condition for impermeable walls reads as

$$\mathbf{v}_\alpha \cdot \mathbf{n} = -\lambda_\alpha (S_\alpha) \mathbf{K} (\nabla p - \rho_\alpha \mathbf{g}) \cdot \mathbf{n} = 0, \quad \alpha \in \{o, g\}, \quad (7)$$

where  $\mathbf{n}$  is the outer normal vector. Consequently, in two-phase region (where  $\lambda_\alpha \neq 0$  for both  $\alpha \in \{o, g\}$ )

$$\nabla p \cdot \mathbf{n} = \rho_o \mathbf{g} \cdot \mathbf{n} \quad \text{and} \quad \nabla p \cdot \mathbf{n} = \rho_g \mathbf{g} \cdot \mathbf{n}, \quad (8)$$

which means that one pressure gradient should equilibrate two different density profiles. This can not be achieved in two-phase problems with gravity and no capillarity unless the two densities are the same. While there is no issue for vertical impermeable walls due to absence of gravity term, the problem appears in the horizontal boundaries. We observe that on the horizontal boundaries we cannot enforce impermeable boundary for both phases. We will see later that it is possible to enforce the normal component of the total molar flux to be zero which is necessary for total mole conservation in the domain, i.e.

$$(c_o \mathbf{v}_o + c_g \mathbf{v}_g) \cdot \mathbf{n} = 0. \quad (9)$$

Equation (9) implies that if one phase is flowing out of the domain, the other phase is flowing in at the same point. The composition and molar density of the inflow phase can be prescribed, while the composition and molar density of the outflow phase is the result of the computation. Therefore, when treating boundary conditions in the transport equations (1), the mole fraction of each component and molar density of the inflow phase are set to the corresponding mole fraction and molar density of the outflow phase, respectively. Note that this problem arises in any discretization scheme for two-phase compositional equations without capillarity and is not connected with the MHFE/DG approach [4].

### 4. Discretization

The system of equations is discretized using the implicit pressure - explicit concentration technique. The pressure equation is discretized by mixed-hybrid finite element method, while the transport equations are discretized using the discontinuous Galerkin finite element method with piecewise linear shape functions on a rectangular grid. The spurious oscillations in the numerical solution are suppressed using the slope limiter.

#### 4.1. Discretization of the total molar flux

The total molar flux is introduced as

$$\mathbf{q} = c_o \mathbf{v}_o + c_g \mathbf{v}_g = - \sum_{\alpha'} c_{\alpha'} \lambda_{\alpha'} \mathbf{K} (\nabla p - \rho \mathbf{g}), \quad (10)$$

where  $\rho = f_o \rho_o + f_g \rho_g$ , and  $f_\alpha = c_\alpha \lambda_\alpha / \sum_{\alpha' \in \{o, g\}} c_{\alpha'} \lambda_{\alpha'}$ . Unlike coefficients  $c_\alpha \lambda_\alpha$  in the phase fluxes, the coefficient  $\sum_{\alpha'} c_{\alpha'} \lambda_{\alpha'}$  in (10) is always positive as at least one of the phases is always mobile. The pressure gradient can then be expressed as

$$\nabla p = - \frac{1}{\sum_{\alpha'} c_{\alpha'} \lambda_{\alpha'}} \mathbf{K}^{-1} \mathbf{q} + \rho \mathbf{g}. \quad (11)$$

Equation (11) can be combined with Darcy’s law given by (2) to obtain the phase molar fluxes

$$\mathbf{q}_\alpha \equiv c_\alpha \mathbf{v}_\alpha = f_\alpha(\mathbf{q} - \mathbf{G}_\alpha), \tag{12}$$

where

$$\mathbf{G}_\alpha = \begin{cases} c_o \lambda_o (\rho_o - \rho_g) \mathbf{K} \mathbf{g} & \alpha = g, \\ c_g \lambda_g (\rho_g - \rho_o) \mathbf{K} \mathbf{g} & \alpha = o. \end{cases} \tag{13}$$

The total molar flux is approximated using the lowest order Raviart-Thomas elements as

$$\mathbf{q}_K = \sum_{E \in \partial K} q_{K,E} \mathbf{w}_{K,E}, \tag{14}$$

where  $q_{K,E}$  is the normal component of the total molar flux over the edge  $E$  of element  $K$  with respect to outer normal, and  $\mathbf{w}_{K,E}$  are the  $RT_0$  basis functions. These functions defined on a reference element  $K = (0, l_x) \times (0, l_y)$  are given by

$$\mathbf{w}_{K,B}(x, y) = \left( 0, \frac{y - l_y}{|K|} \right), \quad \mathbf{w}_{K,T}(x, y) = \left( 0, \frac{y}{|K|} \right), \quad \mathbf{w}_{K,L}(x, y) = \left( \frac{x - l_x}{|K|}, 0 \right), \quad \mathbf{w}_{K,R}(x, y) = \left( \frac{x}{|K|}, 0 \right),$$

where the  $B, T, L,$  and  $R$  denote the bottom, top, left, and right edge in the element  $K$ , respectively. Multiplying (11) by  $\mathbf{w}_{K,E}$ , integrating the result over the element  $K$ , and using the Gauss theorem, one obtains

$$\int_K \frac{\mathbf{w}_{K,E} \cdot \mathbf{K}^{-1} \mathbf{q}}{\sum_{\alpha'} c_{\alpha'} \lambda_{\alpha'}} = - \int_K \mathbf{w}_{K,E} \cdot \nabla p + \int_K \rho \mathbf{w}_{K,E} \cdot \mathbf{g} = \int_K p \nabla \cdot \mathbf{w}_{K,E} - \int_{\partial K} p \mathbf{w}_{K,E} \cdot \mathbf{n}_{K,E} + \int_K \rho \mathbf{w}_{K,E} \cdot \mathbf{K}^{-1} \mathbf{K} \mathbf{g}. \tag{15}$$

The right side can be rewritten as

$$\int_K \frac{\mathbf{w}_{K,E} \cdot \mathbf{K}^{-1} \mathbf{q}}{\sum_{\alpha'} c_{\alpha'} \lambda_{\alpha'}} = \frac{1}{|K|} \int_K p - \frac{1}{|E|} \int_E p + \int_K \rho \mathbf{w}_{K,E} \cdot \mathbf{K}^{-1} \mathbf{K} \mathbf{g}, \tag{16}$$

where  $|K|$  is the area of the element  $K$  and  $|E|$  is the length of the edge  $E$ . Let  $p_K$  and  $tp_{K,E}$  denote the cell and edge average pressure, respectively. Assuming that the mobilities and densities are constant over the element  $K$ , equation (16) is approximated by

$$\sum_{E' \in \partial K} \frac{q_{K,E'}}{\sum_{\alpha'} c_{\alpha'} \lambda_{\alpha',K}} \mathbf{A}_{K,E,E'} = p_K - tp_{K,E} + \sum_{E' \in \partial K} \rho_K q_{K,E'}^{Kg} \mathbf{A}_{K,E,E'}, \tag{17}$$

where

$$\mathbf{A}_{K,E,E'} = \int_K \mathbf{w}_{K,E} \cdot \mathbf{K}_K^{-1} \mathbf{w}_{K,E'}, \quad \text{and} \quad q_{K,E}^{Kg} = \int_E \mathbf{K} \mathbf{g} \cdot \mathbf{n}_{K,E} = \mathbf{K} \mathbf{g} \cdot \mathbf{n}_{K,E} |E|. \tag{18}$$

After inverting the matrix  $\mathbf{A}_K = [\mathbf{A}_{K,E,E'}]_{E,E' \in \partial K}$ , the flux  $q_{K,E}$  can be expressed as

$$q_{K,E} = a_{K,E} p_K - \sum_{E' \in \partial K} b_{K,E,E'} tp_{K,E'} + d_{K,E}, \tag{19}$$

where

$$a_{K,E} = \sum_{\alpha'} c_{\alpha',K} \lambda_{\alpha',K} \sum_{E' \in \partial K} \mathbf{A}_{K,E,E'}^{-1}, \quad b_{K,E,E'} = \sum_{\alpha'} c_{\alpha',K} \lambda_{\alpha',K} \mathbf{A}_{K,E,E'}^{-1}, \quad d_{K,E} = \mathbf{K} \mathbf{g} \cdot \mathbf{n}_{K,E} |E| \sum_{\alpha'} c_{\alpha',K} \lambda_{\alpha',K} \rho_{\alpha,K}. \tag{20}$$

The mole balance at an edge  $E = K \cap K'$  between neighboring elements  $K$  and  $K'$  implies that  $q_{K,E} + q_{K',E} = 0$ . Combining this equation with (19), we derive

$$a_{K,E} p_K - \sum_{E' \in \partial K} b_{K,E,E'} tp_{K,E'} + d_{K,E} + a_{K',E} p_{K'} - \sum_{E' \in \partial K'} b_{K',E,E'} tp_{K',E'} + d_{K',E} = 0, \tag{21}$$

for each interior face. For boundary faces  $E \subset \partial\Omega$  adjacent to an element  $K$ , we use (9) to obtain  $q_{K,E} = 0$ , whence

$$a_{K,E}p_K - \sum_{E' \in \partial K} b_{K,E,E'}tp_{K,E'} + d_{K,E} = 0. \tag{22}$$

The system of equations (21) and (22) can be rewritten in the matrix form as

$$R^T P - MTP = V, \tag{23}$$

where

$$R \in \mathbb{R}^{N_K \times N_E}, R_{K,E} = a_{K,E}, \quad M \in \mathbb{R}^{N_E \times N_E}, M_{E,E'} = \sum_{K: E, E' \in \partial K} b_{K,E,E'}, \quad V \in \mathbb{R}^{N_E}, V_E = \sum_{K: E \in \partial K} d_{K,E}, \tag{24}$$

and  $N_K$  is the number of element cells,  $N_E$  is the number of mesh edges,  $P \in \mathbb{R}^{N_K}$  is the vector of cell-average pressures, and  $TP \in \mathbb{R}^{N_E}$  is the vector of pressure traces.

#### 4.2. Approximation of the pressure equation

The pressure equation given by (3) expressed in terms of the total molar flux reads as

$$\phi c_f \frac{\partial p}{\partial t} + \sum_{i=1}^{n_c} \bar{v}_i \nabla \cdot (m_i \mathbf{q} - \mathbf{s}_i) = \sum_{i=1}^{n_c} \bar{v}_i F_i, \tag{25}$$

where  $m_i = x_{oi}f_o + x_{gi}f_g$ , and  $\mathbf{s}_i = x_{oi}f_o \mathbf{G}_o + x_{gi}f_g \mathbf{G}_g$ . Integrating this equation over an element  $K$  and assuming that the total compressibility and the total partial molar volumes are element-wise constant, we use the divergence theorem to transform the last equation into

$$\phi_K c_{f,K} |K| \frac{\partial p_K}{\partial t} + \sum_{i=1}^{n_c} \bar{v}_{i,K} \sum_{E \in \partial K} \int_E (m_{i,K} q_{K,E} - \mathbf{s}_{i,K} \cdot \mathbf{n}_{K,E}) = \sum_{i=1}^{n_c} \bar{v}_{i,K} F_{i,K} |K|. \tag{26}$$

The coefficients  $m_{i,K}$  and  $\mathbf{s}_{i,K}$  are evaluated using the local average values inside element  $K$ . The flux in this equation can be eliminated using (19). Using the Euler scheme for discretization of the time derivative, in which all composition-dependent coefficients are evaluated explicitly using the values from previous time level while pressure is treated implicitly, we develop the following system

$$DP^{n+1} - \tilde{R}TP^{n+1} = G, \tag{27}$$

where  $n + 1$  denotes the new time level,  $D \in \mathbb{R}^{N_K \times N_K}$  is a diagonal matrix with diagonal components

$$D_K = \frac{\phi_K c_{f,K} |K|}{\Delta t} + \sum_{i=1}^{n_c} \bar{v}_{i,K} \sum_{E \in \partial K} \int_E m_{i,K} a_{K,E},$$

$\tilde{R} \in \mathbb{R}^{N_K \times N_E}$  is a rectangular matrix with components

$$\tilde{R}_{K,E'} = \sum_{i=1}^{n_c} \bar{v}_{i,K} \sum_{E \in \partial K} \int_E m_{i,K} b_{K,E,E'},$$

and  $G \in \mathbb{R}^{N_K}$  is a right side vector with components

$$G_K = \frac{\phi_K c_{f,K} |K|}{\Delta t} p_K^n - \sum_{i=1}^{n_c} \bar{v}_{i,K} \sum_{E \in \partial K} \int_E (m_{i,K} d_{K,E} - \mathbf{s}_{i,K} \cdot \mathbf{n}_{K,E}) + |K| \sum_{i=1}^{n_c} \bar{v}_{i,K} F_{i,K}.$$

### 4.3. Evaluation of the Phase Fluxes

As a result of previous development, we derived a system of linear algebraic equations (23) and (27) for unknown cell pressure averages  $P$  and traces of pressure at the element edges  $TP$  at a new time level. This system can be solved efficiently by taking advantage of the fact that the matrix  $D$  is diagonal and invertible. Therefore, the system can be reduced to a smaller system

$$(M - R^T D^{-1} \tilde{R})TP^{n+1} = R^T D^{-1}G - V. \tag{28}$$

for unknown traces of pressure. Once this system is solved, the cell average pressures  $P$  can be updated using (27) and the total molar flux can be evaluated from (19). All these computations can be done locally on each element.

The next step is the evaluation of the phase fluxes using (12). For this purpose, using local values of  $f_\alpha$  and  $\mathbf{G}_\alpha$  would lead to non-matching phase fluxes at element edges. It has been observed that arithmetic averaging of the coefficients leads to unstable oscillatory results. To obtain stable phase fluxes that are balanced at mesh edges, the values of  $\rho_\alpha$  used in  $\mathbf{G}_\alpha$  in (12) are weighted arithmetically from the neighboring cells, while  $c_\alpha \lambda_\alpha$ , and  $c_{\alpha'} \lambda_{\alpha'}$  in  $f_\alpha$  should be taken from the upwind side with respect to  $\mathbf{v}_\alpha$ , cf. [10]. To determine the upwind directions ( $\mathbf{q}_\alpha$  is not available yet), let us denote by  $\alpha$  the phase for which

$$\text{sgn } \mathbf{q}_{\alpha,K,E} \cdot \mathbf{n}_{K,E} = -\text{sgn } \mathbf{G}_\alpha \cdot \mathbf{n}_{K,E},$$

and let  $\alpha'$  denote the other phase. The choice is always possible because the total flux is already known and vectors  $\mathbf{G}_\alpha$  and  $\mathbf{G}_{\alpha'}$  are pointing in the opposite directions. The sign of  $q_{\alpha,K,E}$  is thus the same as the sign as of  $q_{K,E}$ . This sign does not depend on the value of  $c_{\alpha'} \lambda_{\alpha'}$  in (12), which is unknown but non-negative. Using the known sign of  $q_{\alpha,K,E}$ , we can choose the upwind value of  $c_\alpha \lambda_\alpha$  in the computation of  $\mathbf{G}_{\alpha'}$ . We can thus determine  $q_{\alpha',K,E}$  and finally the value of  $\lambda_{\alpha'}$  is determined and used for evaluation of the final value of  $q_{\alpha,K,E}$ .

### 4.4. Discretization of transport equations

The transport equations (1) are discretized using the discontinuous Galerkin finite element method with element-wise linear approximation of the molar concentration  $cz_i$ . Assuming the approximation in the form

$$cz_{i,K} = \sum_{l=1}^3 cz_{i,K}^l \varphi_{K,l}, \quad x_{\alpha i,K} = \sum_{l=1}^3 x_{\alpha i,K}^l \varphi_{K,l}, \quad \mathbf{q}_{\alpha,K} = \sum_{E \in \partial K} q_{\alpha,K,E} \mathbf{w}_{K,E}, \tag{29}$$

where functions  $\varphi_{K,l}$  form a basis of a local approximation space, we multiply (1) by a test function, integrate over the element  $K$  and integrate by parts to obtain

$$\int_K \phi \frac{\partial cz_{i,K}}{\partial t} \varphi_{K,j} - \int_K (x_{oi,K} \mathbf{q}_o + x_{gi,K} \mathbf{q}_g) \cdot \nabla \varphi_{K,j} + \sum_{E \in \partial K} \int_E (\widetilde{x_{oi,K,E}} \mathbf{q}_o + \widetilde{x_{gi,K,E}} \mathbf{q}_g) \cdot \mathbf{n}_{K,E} \varphi_{K,j} = \int_K F_i \varphi_{K,j}, \tag{30}$$

for each  $j \in \{1, 2, 3\}$ . The  $\widetilde{x_{\alpha i,K,E}}$  ( $\alpha \in \{o, g\}$ ) denotes the upwind value of concentration defined as

$$\widetilde{x_{\alpha i,K,E}} = \begin{cases} x_{\alpha i,K,E} & \text{if } q_{\alpha,K,E} \equiv \mathbf{q}_\alpha \cdot \mathbf{n}_{K,E} |E| \geq 0, \\ x_{\alpha i,K',E} & \text{if } q_{\alpha,K,E} \equiv \mathbf{q}_\alpha \cdot \mathbf{n}_{K,E} |E| < 0, \end{cases} \tag{31}$$

where  $E = K \cap K'$  is a common edge between the neighboring elements  $K$  and  $K'$ . For boundary edges, the Dirichlet boundary conditions on the influx part of the boundary are applied. The values  $x_{\alpha i,K,E}$  and  $x_{\alpha i,K',E}$  in (31) are computed by two-phase flash at element edges using the values of  $T$ ,  $TP$  and  $z_i$  at that edge. The values  $x_{\alpha i,K}$  in the second integral on the left hand side of (29) are evaluated by the two-phase flash using the values of  $T$ ,  $P$  and  $z_i$  at the element center. Altogether 5 flashes are performed on each element. Substitution of (29) into (30) results in the following semi-discrete scheme

$$\phi_K \sum_{l=1}^3 \frac{dcz_{i,K}^l}{dt} M_{j,l}^K - \sum_{\alpha \in \{o,g\}} \sum_{l=1}^3 x_{\alpha i,K} \sum_{E \in \partial K} q_{\alpha,K,E} M_{j,l}^{K,E} + \sum_{E \in \partial K} \sum_{\alpha \in \{o,g\}} \widetilde{x_{\alpha i,K,E}} q_{\alpha,K,E} M_j^E = \int_K F_i \varphi_{K,j}. \tag{32}$$

The matrices  $M^K$ ,  $M^E$ , and  $M^{K,E}$ , defined by

$$M_{j,l}^K = \int_K \varphi_{K,j} \varphi_{K,l}, \quad M_j^E = \frac{1}{|E|} \int_E \varphi_{K,j}, \quad M_{j,l}^{K,E} = \int_K \varphi_{K,l} \mathbf{w}_{K,E} \cdot \nabla \varphi_{K,j},$$

can be evaluated analytically. For linear test functions  $\varphi_{K,l}$  defined on a reference element  $K = (0, l_x) \times (0, l_y)$  by

$$\varphi_{K,1}(x, y) = 1, \quad \varphi_{K,2}(x, y) = \frac{2}{l_x} \left( x - \frac{l_x}{2} \right), \quad \varphi_{K,3}(x, y) = \frac{2}{l_y} \left( y - \frac{l_y}{2} \right), \quad (33)$$

the weighting factors  $cz_{i,K}^l$  ( $l = 1, 2, 3$ ) are the average value of molar concentration over the element  $K$ , and differences between the central value and the values at the right and top edges, respectively. For these test functions the matrix  $M^K$  is diagonal, and the forward Euler scheme leads to an explicit scheme in terms of  $cz_{i,K}^l$  with 3 degrees of freedom on each element.

The discontinuous Galerkin method, similarly as any other high resolution method, has to be stabilized to avoid spurious oscillations of the numerical solution using a slope limiter. On rectangular grids the slopes in the horizontal and vertical directions can be limited independently of each other. After each step of DG method the limiter provides bounds  $cz_{i,min}$  and  $cz_{i,max}$  at each edge  $E$  by taking minimum and maximum of  $cz_{i,K}$  over elements  $K$  sharing the edge  $E$ . If needed, the slopes may be decreased in the absolute value so that the inequalities

$$cz_{i,min} \leq cz_i \leq cz_{i,max} \quad (34)$$

hold at every edge  $E$  for each  $i = 1, \dots, n_c$ . It is important to note that this limiting procedure works well only if used for the original system of equations (1) for each  $i = 1, \dots, n_c$ . If a commonly used formulation using (1) for  $i = 1, \dots, n_c - 1$  and the sum of all equations (1) is used, the limiter provides bounds  $cz_{i,min}$  and  $cz_{i,max}$  for  $i = 1, \dots, n_c - 1$  and bounds for total concentration  $c_{min}$  and  $c_{max}$ . The implied bounds on the concentration of the last component  $cz_{n_c}$  are then  $c_{max} - \sum_{i=1}^{n_c-1} cz_{i,min} \leq cz_{n_c} = c - \sum_{i=1}^{n_c-1} cz_i \leq c_{max} - \sum_{i=1}^{n_c-1} cz_{i,min}$ . These bounds are inconsistent with the bounds given by equation (34) for  $i = n_c$  and lead to spurious oscillations in the concentration profiles which eventually cause the code to crash when an unphysical value of concentration appears [4].

## 5. Computational Algorithm

Here we summarize the basic steps of the computational algorithm:

1. Initialize temperature and distribution of pressure and overall molar concentrations of all components.
2. Perform the phase stability and flash calculations to obtain number of phases and phase compositions at the initial pressure, temperature, and overall composition at element centers and at element faces and evaluate the phase viscosities using the Lohrenz et al. method.
3. Repeat the following steps until a predetermined simulation time is reached.
  - (a) Assemble and solve the system (28) for traces of pressure  $TP$ .
  - (b) Evaluate cell average pressures  $P$  locally on each element using (27).
  - (c) Calculate fluxes using the procedure described in section 4.3.
  - (d) Compute new overall composition using one explicit Euler time step of the DG scheme (32).
  - (e) Apply the slope limiter.
  - (f) Perform the phase stability analysis and flash calculation to obtain number of phases and phase composition at the new pressure, overall composition and temperature  $T$  at element centers and at element faces, and update phase viscosities.

## 6. Numerical Simulations of CO<sub>2</sub> Injections in Oil Reservoirs

In this section, we present results of several simulations computed using the combined MHFE/DG method described above. The results will be compared to those obtained by the same procedure in which the traditional first-order finite volume scheme is used rather than the discontinuous Galerkin (denoted as MHFE/FV). In this case there is no need to assemble equations for the concentration gradients, which are zero, and only 1 flash per element is performed. All the problems were solved on a 2-D square domain  $50 \times 50$  m with a rectangular grid on a HP xw9400 RedHat WS 4 workstation with the Dual-Core AMD Opteron 2216 CPU at 2.4GHz and 4GB memory. The relevant parameters for all examples are summarized in Table 1.

Soil and mixture parameters		Component parameters	CO <sub>2</sub>	propane (C <sub>3</sub> )
Porosity $\phi$	0.2	acentric factor $\omega$	0.239	0.153
Permeability $\mathbf{K}$ [md]	10	critical temperature $T_c$ [K]	304.14	396.83
Relative permeability model type	linear	critical pressure $P_c$ [bar]	73.75	42.48
Residual gas saturation $S_{rg}$	0	critical volume $v_c$ [m <sup>3</sup> /kg]	0.00214	0.00454
Residual oil saturation $S_{ro}$	0	molar weight $M$ [g/mol]	44	44.1
Binary interaction parameter $\delta_{CO_2-C_3}$	0.15	volume shift parameter $c$	-0.18	-0.09

Table 1: Relevant parameters for all simulations. The notation of parameters of the Peng-Robinson equation of state follows the exposition in [8].

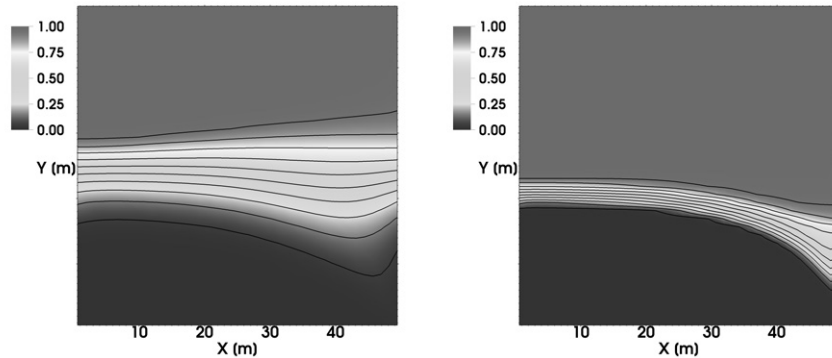


Figure 1: CO<sub>2</sub> mole fraction at 0.56 years computed on a 40 × 40 mesh by the MHFE/FV (left) and the MHFE/DG methods (right): Example 1

### 6.1. Example 1

In this example we simulate injection of CO<sub>2</sub> into a propane-saturated reservoir in a vertical 2D domain. CO<sub>2</sub> is injected in the upper left corner at a constant rate (corresponding to 42.5 m<sup>2</sup>/day at standart conditions  $p = 1$  atm and  $T = 293$  K), displacing propane that is produced in the lower right corner. Pressure at the production well is kept constant at  $p = 69$  bar, temperature in the whole domain is  $T = 311$  K. Under these conditions the mixture stays in single-phase during whole simulation. Figure 1 shows CO<sub>2</sub> mole fraction at 66% of PVI computed using the MHFE/DG and MHFE/FV methods on a 40 × 40 mesh. The computation time (to 100% PVI) is 2 minutes for both methods. We observe the excessive numerical dispersion in the finite-volume method compared to the DG. To see better the effect of numerical diffusion, the black lines in all figures show the isolines with values 0.05, 0.15, 0.25, . . . , 0.95.

### 6.2. Example 2

In the second example we change the pressure in Example 1 to allow for two-phase flow. CO<sub>2</sub> is injected in the upper left corner at the same rate as in Example 1, but the mixture is produced in the lower right corner at lower pressure  $p = 25$  bar. Temperature and other parameters are the same as in Example 1. Under lower pressure the mixture splits into two phases. Figures 2 and 3 show CO<sub>2</sub> mole fraction and gas phase saturation profiles at 66% of PVI computed using the MHFE/DG and MHFE/FV methods on a 40 × 40 mesh. The computation time (to 100% PVI) is 2 minutes for both methods. The reduction of the excessive numerical diffusion in the MHFE/DG method is significant even in the two-phase case. Less numerical diffusion in MHFE/DG method also influences the position of the saturation front, see Figure 3.

### 6.3. Example 3

In the last example we simulate the injection of CO<sub>2</sub> in the vertical 2D domain in which CO<sub>2</sub> is injected at the bottom left corner at the same rate as before and the mixture is produced in the upper right corner. The pressure in the production well is  $p = 69$  bar and the temperature in the whole domain is  $T = 311$  K. Under these conditions the mixture stays in single-phase. Figure 4 shows the mole fraction of CO<sub>2</sub> at PVI=50% computed by both methods on a

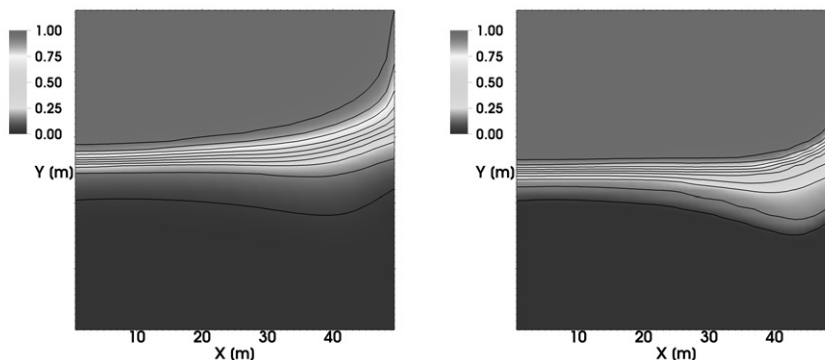


Figure 2: CO<sub>2</sub> mole fraction at 0.56 years computed on a 40 × 40 mesh by the MHFE/FV (left) and the MHFE/DG methods (right): Example 2

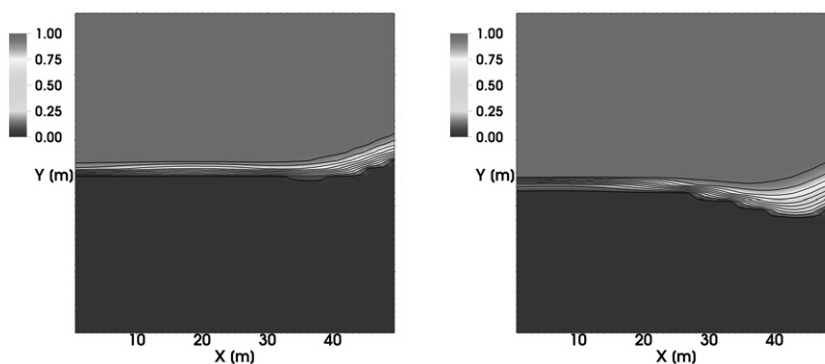


Figure 3: Gas saturation at 0.56 years computed on a 40 × 40 mesh by the MHFE/FV (left) and the MHFE/DG methods (right): Example 2

40 × 40 mesh. As the mixture of CO<sub>2</sub> with propane has lower density than propane, we can observe unstable fingering of CO<sub>2</sub> towards the production well in the MHFE/DG method. This effect is not captured by the MHFE/FV method in which the fingers are suppressed by the strong numerical diffusion. The CPU time to reach PVI=50% is 18 min for the MHFE/FV and 20 min for the MHFE/DG method. The results of the same computation using the MHFE/DG method on finer meshes are shown in Figure 5. The computational time of the MHFE/DG method on the 60 × 60 mesh is 2h 9 min and 8h 2 min on the 80 × 80 mesh. The CPU time for the MHFE/FV method is 1h 51 min on the 60 × 60 mesh and 7h 50 min on the 80 × 80 mesh. The results of the MHFE/FV on 60 × 60 and 80 × 80 meshes are very similar to the result in Figure 4 on the left and are not presented here for brevity.

## 7. Conclusions

In this paper we have discussed formulation of the compressible two-phase compositional flow model. Using high-resolution methods, we construct a numerical model that provides a non-oscillatory solution that contains much less numerical diffusion compared to the traditional first-order schemes. Consequently, the solution obtained using the combined MHFE/DG method exhibits much sharper fronts even on coarse meshes and unlike the MHFE/FV, the MHFE/DG method also captures fingering phenomenon in the physically unstable configuration. In all simulations the CPU time of the MHFE/DG scheme is only slightly longer than of the MHFE/FV method. Although the CPU time is dominated by the flash calculation, the increased number of flashes per element in the MHFE/DG scheme does not increase the CPU time considerably. This can be explained by the fact that the result of the flash on element center provides an excellent initial estimate for the subsequent flashes on element edges. Convergence of the edge flashes is thus much faster in comparison with the flash computations in the element centers.

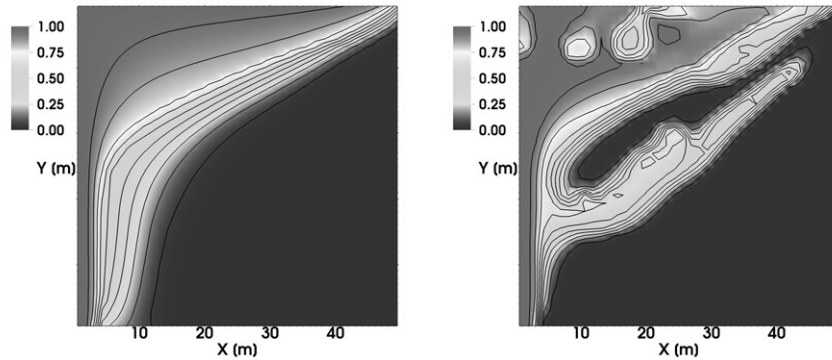


Figure 4: CO<sub>2</sub> mole fraction at 0.18 years computed on a 40 × 40 mesh by the MHFE/FV (left) and the MHFE/DG methods (right): Example 3

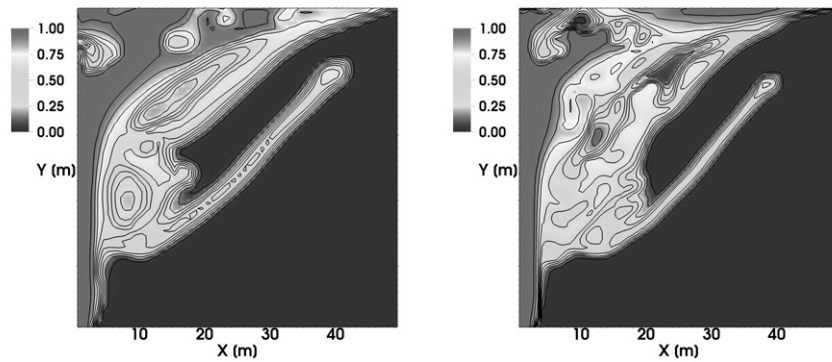


Figure 5: CO<sub>2</sub> mole fraction at 0.18 years computed by the MHFE/DG method on a 60 × 60 (left) and a 80 × 80 mesh (right): Example 3

## Acknowledgements

This work was supported by the member companies of the Reservoir Engineering Research Institute (RERI), and by the project number P105/11/1507 of the Czech Science Foundation.

## References

- [1] H. Hoteit, A. Firoozabadi, Multicomponent fluid flow by discontinuous Galerkin and mixed methods in unfractured and fractured media, *Water Resources Research* 41 (11) (2005) 1–15.
- [2] H. Hoteit, A. Firoozabadi, Compositional modeling of discrete-fractured media without transfer functions by the discontinuous Galerkin and mixed methods, *SPE Journal* 11 (3) (2006) 341–352.
- [3] H. Hoteit, A. Firoozabadi, Compositional modeling by the combined discontinuous Galerkin and mixed methods, *SPE Journal* 11 (1) (2006) 19–34.
- [4] J. Mikyška, A. Firoozabadi, Implementation of higher-order methods for robust and efficient compositional simulation, *Journal of Computational Physics* 229 (8) (2010) 2898–2913. doi:10.1016/j.jcp.2009.12.022.
- [5] J. Moortgat, A. Firoozabadi, Higher-order compositional modeling with Fickian diffusion in unstructured and anisotropic media, *Advances in Water Resources* 33 (9) (2010) 951–968. doi:10.1016/j.advwatres.2010.04.012.
- [6] J. Lohrenz, B. Bray, Clark, Calculating viscosities of reservoir fluids from their compositions, *Journal of Petroleum Technology* 16 (10) (1964) 1171–1176.
- [7] G. Acs, S. Doleschall, E. Farkas, General-Purpose Compositional Model, *SPE Journal* 25 (4) (1985) 543–553.
- [8] A. Firoozabadi, *Thermodynamics of Hydrocarbon Reservoirs*, McGraw-Hill, 1999.
- [9] D. Peng, D. Robinson, New 2-Constant Equation of State, *Industrial & Engineering Chemistry Fundamentals* 15 (1) (1976) 59–64.
- [10] P. Sammon, An analysis of upstream differencing, *SPE Reservoir Engineering* (August) (1988) 1053–1056.